ACS OMEGA

Open Access

http://pubs.acs.org/journal/acsodf

Article

In Vitro and In Vivo Comparison of Random versus Site-Specific Conjugation of Bifunctional Chelating Agents to the CD33-Binding Antibody for Use in Alpha- and Beta-Radioimmunotherapy

Kevin J. H. Allen,[‖] Connor Frank,[‖] Rubin Jiao, Mackenzie E. Malo, Michele Bello, Laura De Nardo, Laura Meléndez-Alafort, and Ekaterina Dadachova*

Cite This: *ACS Omega* 2024, 9, 50000−50011

Read Online

ACCESS | Metrics & More | Article Recommendations | Supporting Information

ABSTRACT: Radiometal chelator conjugation is a cornerstone of radioimmunotherapy (RIT). Continued interest in selective placement of chelators remains an active topic of discussion in the field. With several simple site-specific methods being recently reported, it was of interest to investigate the benefits and potential drawbacks of the site-specific method with a full comparison to a more typical random conjugation method that is currently utilized in clinical applications. In this study, the conjugation methods were evaluated side by side to determine the utility of both methods using commercially available random and site-specific conjugation reagents by performing antigen binding; radiolabeling with ^{64}Cu, ^{177}Lu, and ^{225}Ac radioisotopes; antibody-conjugate stability, cytotoxicity, in vivo distribution, pharmacokinetics analyses, and dosimetry to gather a whole data set for preclinical investigation. Evaluation revealed that both methods performed similarly during most experiments with the site-specific method, resulting in higher binding capacity of the antibody conjugate via flow cytometry. Radiolabeling was not significantly different between two methods, while stability showed that the site-specifically conjugated antibody was somewhat more stable at 37 °C in human serum over 1 week. In vitro experiments demonstrated less cell killing with the random conjugation method, while in vivo experiments showed no statistical differences in tumor uptake between conjugation methods. Dosimetry calculations were performed using the acquired PET/CT data and showed that apart from the liver, there was no significant difference in radiation doses delivered by either antibody conjugate. These results demonstrate that both methods are viable for future work, while the site-specific method offers several potential advantages and, in some cases, improved efficacy.

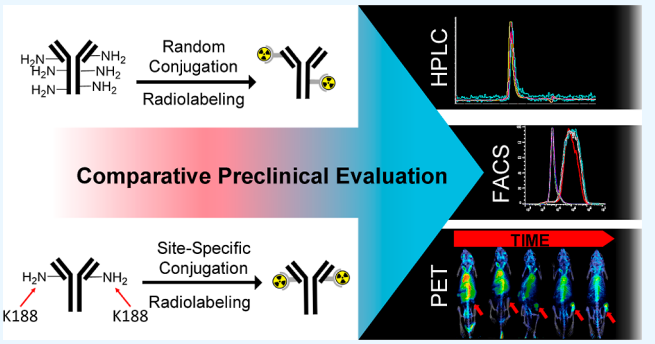

INTRODUCTION

An emerging weapon in the anticancer arsenal is radioimmunotherapy (RIT). RIT exploits the powerful antigen targeting ability of antibodies to deliver cytotoxic radiation to its target antigen.[1] A key requirement in this approach is the ability to attach the radioisotope in a manner that does not hinder the targeting ability of the antibody. The common approach is to utilize chelators that have been modified with a para-isothiocyanatobenzyl moiety (p-SCN-Bn) that can quickly and efficiently bind to any available lysine residue in a random manner.[2] The chelator to antibody ratio (CAR) must be strictly controlled to avoid overloading the antibody with chelator molecules in the binding region that can have adverse effects on the biological effectiveness of each antibody tested.[2] Different approaches have been developed to make the chelator attachment specific to the Fc region of an antibody, namely, enzymatic conjugation[3] and genetic modification of antibodies to include non-natural amino acids that can be exploited for targeted attachment.[2,4] Recently, a chemoselective method that exploits the increased reactivity of K188, a conserved lysine residue found in the constant region kappa light chain that it is conserved across all κ IgG1 antibodies,[5,6] has been reported. Baht et al. first exploited this reactivity using pentafluorophenyl ester (PFP) bifunctional agents,[7] which was then expanded by Sarrett et al. to include the metal chelator deferoxamine, which is capable of binding ^{89}Zr, a common and readily available PET isotope.[5]

This method is potentially attractive as the conjugation of a chelator is divided into two steps: first, site-specific alkyne incorporation and second, strain-promoted azide−alkyne cycloaddition (SPAAC) of a metal chelator in a "click" reaction. This allows for the ability to change the metal

Received: October 16, 2024
Revised: November 18, 2024
Accepted: November 22, 2024
Published: December 4, 2024

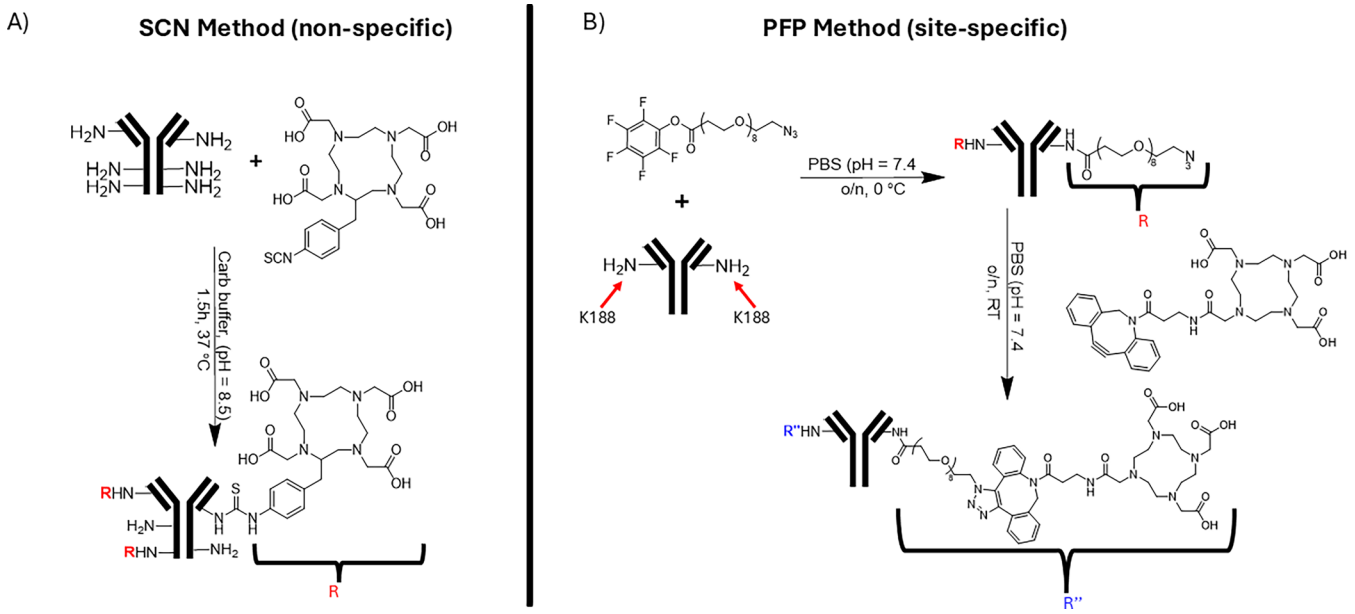

Figure 1. Conjugation of (A) nonspecific, p-SCN-Bn, and (B) site-specific, PFP, functionalized DOTA to an antibody molecule.

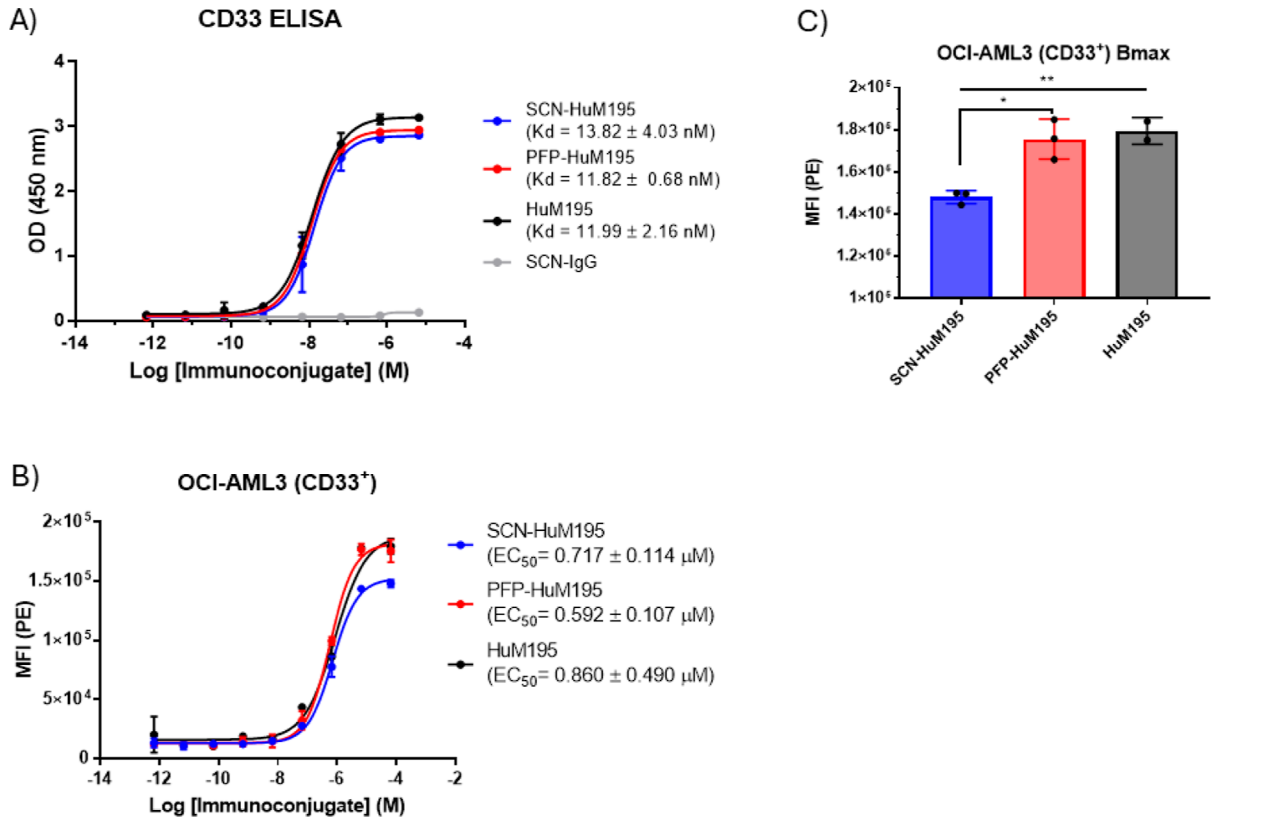

Figure 2. Immunoreactivity and binding data of modified HuM195 immunoconjugates. (A) Indirect enzyme linked immunosorbent assay (ELISA) of HuM195 immunoconjugates against recombinant human Siglec-3 (CD33). (B) Titration flow cytometry binding of HuM195 immunoconjugates to OCI-AML3 cells. (C) Comparison of the total binding capacity (Bmax) of immunoconjugates to that of naïve HuM195. (D) Binding curve of HuM195 immunoconjugates to Daudi cells as a negative control. Flow cytometry controls shown in Supporting Information Figure S1.

chelator as desired without any alterations to the site-specific chemistry.[8]

The aim of this study was to evaluate the impact of this method on a RIT clinically relevant antibody, HuM195 (lintuzumab), which targets CD33, an antigen overexpressed in acute myeloid leukemia. Additionally, the goal was to use commercially available precursors to demonstrate the ease of method implementation. Lastly, to gather a full picture of any differences that can arise from changing conjugation methods, a wide array of standard preclinical screening, such as

https://doi.org/10.1021/acsomega.4c09450
ACS Omega 2024, 9, 50000−50011

Table 1. Radiolabeling Yields for ^{225}Ac-, ^{64}Cu-, and ^{177}Lu-Labeled HuM195 Conjugates

antibody	labeling (%)				
	^{225}Ac		^{64}Cu	^{177}Lu	
	0.037:1 MBq/μg	0.37:1 MBq/μg	0185:1 MBq/μg	10:1 μCi: μg	5:1 μCi: μg
PFP-HuM195	97.5 ± 2	98.1 ± 1.5	>99%	99.2 ± 0.5	>99%
SCN-HuM195	96 ± 2.5	97.3 ± 1.3	>99%	99.0 ± 0.5	>99%

bioreactivity, labeling efficacy, in vitro and in vivo efficacy, and dosimetry, was performed to elucidate these disparities.

RESULTS AND DISCUSSION

The reliability and reproducibility of antibody-chelator conjugation are cornerstones for the development of radiopharmaceutical therapeutics. One approach to enhancing reproducibility is a site-specific conjugation.[2,4,9,10] The advantage of these methods is that they target very specific regions on antibodies, eliminating the randomness associated with the commonly used method that employs a para-isothiocyanate benzyl moiety, which can react with any chemically available lysine, including those on the antibody complementarity determining region (CDR). The traditional method's drawback is the potential for targeting a lysine that hinders antigen recognition, thereby decreasing immunoreactivity.[2,5]

To investigate the potential benefits of a site-specific method, we directly compared a clinically relevant antibody, HuM195, conjugated using the random p-SCN-Bn method (Figure 1A) to a recently published site-specific PFP method.[5] This method exploits the heightened reactivity of K188 residues on the kappa light chain of the IgG1 antibodies. Unlike the proprietary azido-PEG-PFP-ester used in the literature example,[5] we employed a commercially available azido-PEG8-PFP-ester to ensure broad accessibility. The PEG chain length was selected to maximize the distance of the reactive azide from the antibody, fully exposing it for SPAAC. For the SPAAC reagent, we used commercially available DO3A-DBCO (Figure 1B). While not completely analogous to DOTA as one of the carboxylic acid pendant arms is replaced with a bifunctional chelating moiety, which can reduce its coordination number, DO3A is expected to have a similar serum stability profile for ^{225}Ac,[11] a clinically promising alpha-particles emitting radioisotope.[12−16]

This method was investigated primarily for its simplicity in incorporating chelators into a wide range of antibodies, compared to other site-specific methods that require multiple enzymes, which can compromise antibody integrity, or necessitate the inclusion of non-natural amino acids into the antibody sequence.[2] To evaluate the specificity of this method, matrix-assisted laser desorption/ionization mass spectrometry (MALDI-MS) analysis was performed, showing a CAR of 2.4. Theoretically, a maximum of two conjugates can be added to the antibody by using this method. This is achieved by increasing the reactivity of K188 relative to other lysine residues in the antibody. To exploit this reactivity, conjugation is performed at a reduced temperature to limit the reactivity of other lysine residues. Our experiment was conducted in a 4 °C "cold" room, with such facilities being widely available at biomedical research institutions, whereas the literature suggests that a temperature closer to 0 °C could further improve selectivity, potentially explaining the slight increase in conjugate incorporation.

To modulate the CAR using the p-SCN-Bn method, reactions were performed with varying molar excesses of bifunctional conjugates. MALDI-MS analysis of 10-fold and 20-fold molar excess yielded CARs of 4.5 and 8.7, respectively. Since the molecular weights of the 10-fold excess p-SCN-Bn conjugates and those produced by PFP were found to be highly comparable (149 850 vs 149 891 Da), the 10-fold excess conjugate was chosen for comparison to the site-specific method.

To assess any potential differences in immunoreactivity between the modified immunoconjugates, both recombinant protein ELISA and cell flow cytometry were conducted (Figure 2). The results showed modest changes in the K_d values between the antibody conjugates and the unmodified antibody. A slightly reduced dissociation constant between the site-specific conjugate and the p-SCN-Bn method was observed with K_d values of 11.8 vs 13.8 nM, respectively; this difference was however not statistically significant (p = 0.1894, Figure 2A). There was also no difference detected between PFP and unconjugated HuM195 (K_d 11.82 vs 11.99, respectively, p = 0.9828).

Flow cytometry data demonstrated no significant difference in EC_{50} values using the p-SCN-Bn conjugate versus PFP site-specific modification (0.592 vs 0.717 μM, respectively, Figure 2B). Decreased binding capacity (Bmax) of the p-SCN-Bn conjugate was observed compared to PFP site-specific modification and unconjugated HuM195 (p = 0.0106 and 0.0096, respectively) (Figure 2C). Taken together, these results demonstrate similar immunoreactivity and binding performances of site-specifically modified and traditional SCN conjugated antibodies. p-SCN-Bn conjugation performed slightly worse with lowered binding capacity on live cells with limited effect on affinity (Figure 2B). This could be due to steric or electrostatic hindrances in the bifunctional chelator moieties. The length of the chelators chosen also could influence the total binding capacity. The longer PEGylated DO3A moiety employed for PFP site-specific applications offers a greater distance from the antibody, thereby reducing the potential interference of binding when the antibody is clustered closely during antigen binding. OCI-AML3 is reported to contain approximately ∼2000 CD33 antigens/cell, potentially leading to saturation and interference of antibodies labeling the surface of the cell.[17]

Ideally, a minimal impact on biological effectiveness is desired with conjugate incorporation. However, the efficacy of radioisotopic labeling becomes crucial when determining the optimal CAR for the p-SCN-Bn method. Evaluation of labeling efficacy revealed no significant difference at 0.185:1 and 0.37:1 MBq/μg specific activity, with both methods achieving near-quantitative labeling for ^{177}Lu and ^{64}Cu and at a 0.037:1 MBq/μg for ^{225}Ac (Table 1). While variations may arise at higher specific activity levels, these results were encouraging that both methods are viable for RIT development. Additionally, size exclusion chromatography (SEC) high-performance liquid chromatography (HPLC) analysis was performed on ^{64}Cu-,

https://doi.org/10.1021/acsomega.4c09450
ACS Omega 2024, 9, 50000−50011

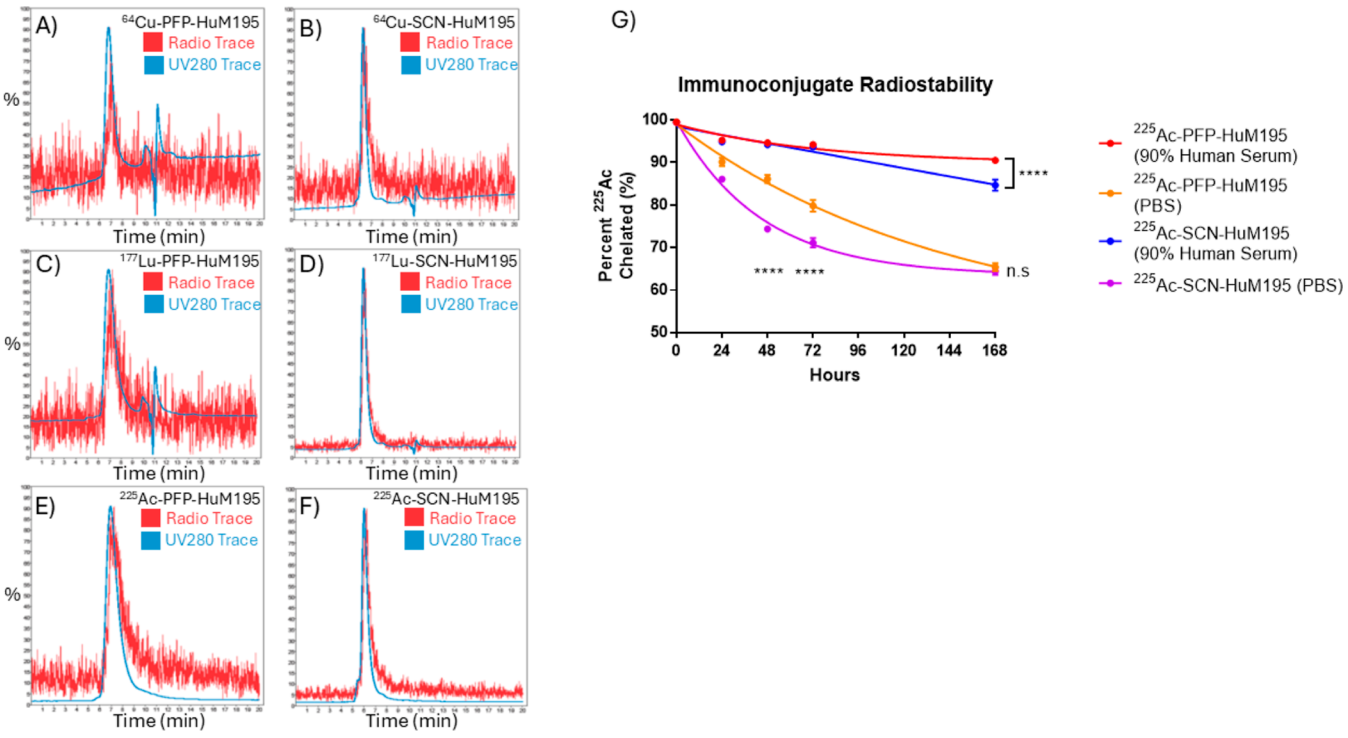

Figure 3. RadioHPLC and stability evaluation of radiolabeled PFP-HuM195 and SCN-HuM195 immunoconjugates. HPLC chromatograms run at a wavelength of 280 nm (blue) and radioactive trace (red). (A,B) ^{64}Cu-PFP-HuM195 and ^{64}Cu−SCN-HuM195; (C,D) ^{177}Lu-PFP-HuM195 and ^{177}Lu-SCN-HuM195; (E,F) ^{225}Ac-PFP-HuM195 and ^{225}Ac-SCN-HuM195; and (G) stability over 7 days for ^{225}Ac-PFP-HuM195 and ^{225}Ac-SCN-HuM195 in human serum and PBS.

^{177}Lu-, and ^{225}Ac-labeled antibodies (Figure 3A−F). This revealed that both antibody conjugates remained intact during the labeling process, with no significant aggregation or degradation observed.

The stability of both^{225}Ac-labeled conjugates were tested in PBS and human serum (Figure 3G). Both ^{225}Ac-PFP-HuM195 and ^{225}Ac-SCN-HuM195 conjugates were highly stable in human serum for the first 72 h, remaining over 94% intact with no significant difference observed between the two methods. Such similarity is expected as DO3A and DOTA have been reported to have similar binding affinities for ^{225}Ac.[11] By day 7, stability showed a significant difference of 90.5 ± 0.5% and 84.7 ± 1.3% for ^{225}Ac-PFP-HuM195 and^{225}Ac-SCN-HuM195, respectively, indicating that there may be linker kinetics involved with the slightly worse stability of the p-SCN-Bn conjugate. In pure PBS, stability was significantly reduced for^{225}Ac-SCN-HuM195 and ^{225}Ac-PFP-HuM195 as early as 24 h (Figure 3G) compared to those stored in human serum. Interestingly, by 48 h, there were significant differences between the two conjugates stored in PBS that persisted to at least 72 h. By 7 days, however, the stability curves coalesced, resulting in both samples remaining only 64.4% ± 0.9 and 65.5% ± 0.9 intact with no significant difference between them. The data demonstrate that if the conjugates are to be shipped radiolabeled overnight, a stabilizing agent such as human serum albumin must be added to maintain the intactness of the radiolabeled conjugates.

The cytotoxic potentials of site-specific PFP modified and p-SCN-Bn conjugated HuM195 was assessed using the α particle emitter ^{225}Ac (Figure 4A−C and Supporting Information Figure S2). Calculated IC_{50} values align with the cell-based binding assays, demonstrating a slightly lower IC_{50} value for the p-SCN-Bn compared to the PFP-modified HuM195 (7.57 vs 4.54 kBq, Figure 4D). There was a significant difference in the cytotoxicity curves, which exhibited a dose-dependent trend. The higher activities (18.5 and 4.63 kBq) of ^{225}Ac-PFP-HuM195 demonstrated a larger amount of cell death over time compared to the same dose of ^{225}Ac-SCN-HuM195 (p = 0.0081, both high and medium dose, Figure 4A,B). A low dose of ^{225}Ac labeled immunoconjugates showed no difference in cytotoxicity (0.29 kBq, Figure 4C). A saturating dose (37 kBq) of ^{225}Ac labeled immunoconjugates demonstrated a threshold where no detectable difference in cytotoxicity was observed between the two immunoconjugates (Figure 4E). Both ^{225}Ac labeled HuM195 immunoconjugates at 37 kBq almost completely inhibited the replication potential of $CD33^+$ OCI-AML3 cells over 72 h compared to untreated controls (Figure 4E). These results in conjunction with the cell binding and immunoreactivity data suggest that the reduced binding capacity of the p-SCN-Bn conjugate resulted in a moderate reduction of payload delivery. In vitro evaluation of cytotoxicity values demonstrates a 34% reduced IC_{50} constant for the p-SCN-Bn conjugate compared to the PFP conjugate (Figure 4D). Arguably, this may result in a larger amount of p-SCN-Bn conjugate being needed to overcome the reduction in payload delivery compared with the PFP conjugation method. Interestingly, the attachment of DOTA chelator via either the p-SCN-Bn or PFP method did not affect the internalization of the HuM195 antibody into the CD33+ OCI-AML3 cells (Figure 4F).

To understand better how each conjugation method performed in a more complex biological system, mice were implanted with human acute myeloid leukemia OCI-AML3 xenografts (n = 4/group). Both PFP-HuM195 and SCN-

https://doi.org/10.1021/acsomega.4c09450
ACS Omega 2024, 9, 50000−50011

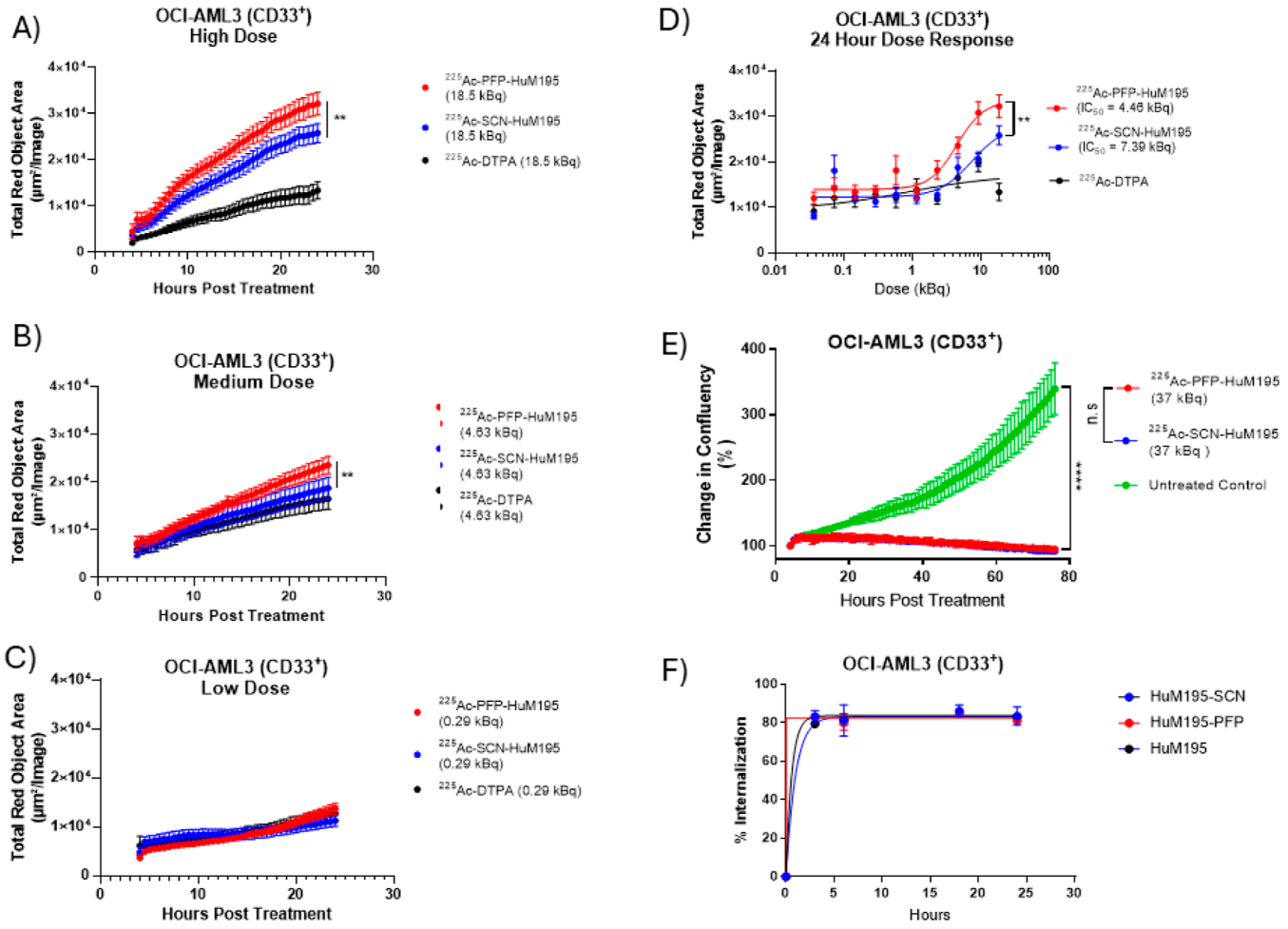

Figure 4. Internalization into OCI-AML3 and in vitro cytotoxicity data of ^{225}Ac-labeled HuM195 immunoconjugates and free ^{225}Ac-DTPA control against OCI-AML3 cells. (A−C) Cytotoxicity curves for high (18.5 kBq), medium (4.63 kBq), and low dose (0.29 kBq) of ^{225}Ac-labeled HuM195 immunoconjugates against CD33$^+$ cells over 24 h. (D) 24 h dose−response curve of ^{225}Ac-labeled HuM195 immunoconjugates against OCI-AML3 cells with calculated inhibitory constant (K_i) values. (E) Comparison of ^{225}Ac-labeled HuM195 immunoconjugates effect on cell confluency compared to untreated control; and (F) internalization of HuM195 and of immunoconjugates into OCI-AML3 cells.

HuM195 were labeled with ^{64}Cu, a positron-emitting isotope. Their microPET/CT images were then utilized to facilitate a comparative analysis of their biodistribution and to generate their respective biokinetic curves. The source organs (SOs) (heart, kidney, liver, spleen, and intestine) were identified based on the hot spots observed in the 3D reconstruction PET images (Figure 5A,B). Subsequently, the biodistribution of each conjugate was determined by calculating the standardized uptake values (SUVs), expressed as percent injected activity per gram of tissue (% IA/g), for each SO and time point. The biodistribution data obtained from the micro-PET/CT images at 44 h were found to be comparable to those obtained from ex vivo studies at the same time (Figure S3), indicating that the imaging analysis method used was accurate. The results of the multiple paired *t*-test statistical analysis, which was used to compare the biodistribution of the two HuM195 conjugates, indicated that the only statistically significant differences were observed in liver uptake at the 5 h time point (p-value = 3.81×10^{-4}, q-value = 1.53×10^{-3}). No other statistically significant differences were identified in the conjugate's uptake in other organs at any time point.

The kinetic curves, generated from the biodistribution data, revealed that the conjugates exhibited rapid blood clearance within the first hour, followed by a significantly slower rate of elimination from the bloodstream (Figure 6). The SCN-HuM195 conjugate showed higher concentrations in the liver and kidney during the initial 5 h, followed by a gradual decline. Clearance of both HuM195 conjugates from other organs was markedly slow, likely due to their elevated concentration in the blood. Tumor kinetic curves indicated that the concentration of SCN-HuM195 exceeded that of PFP-HuM195 after injection; however, this difference in concentration disappeared after 42 h.

To ensure that antigen selectivity was conserved, two of the four mice groups (n = 8) were injected with 0.5 mg of unmodified HuM195 24 h prior to the radiolabeled conjugate (blocked) (Figure 5C,D), while two groups were left unblocked (Figure 5A,B). By injecting a large amount of "cold" antibody to block the target antigen, a decrease in tumor uptake relative to an unblocked tumor would be expected if specificity is conserved. ^{64}Cu-PFP-HuM195 and ^{64}Cu−SCN-HuM195 were injected in both a blocked and unblocked group, with each group being imaged at 1, 5, 20, 30, and 44 h post injection. Postimaging analysis was performed by manually segmenting each tumor and comparing the standardized uptake value normalized by body weight (SUVbw) between each imaging time point (Figure 7). Initial time points, 1 and 5 h, showed little difference between tumor

https://doi.org/10.1021/acsomega.4c09450
ACS Omega 2024, 9, 50000−50011

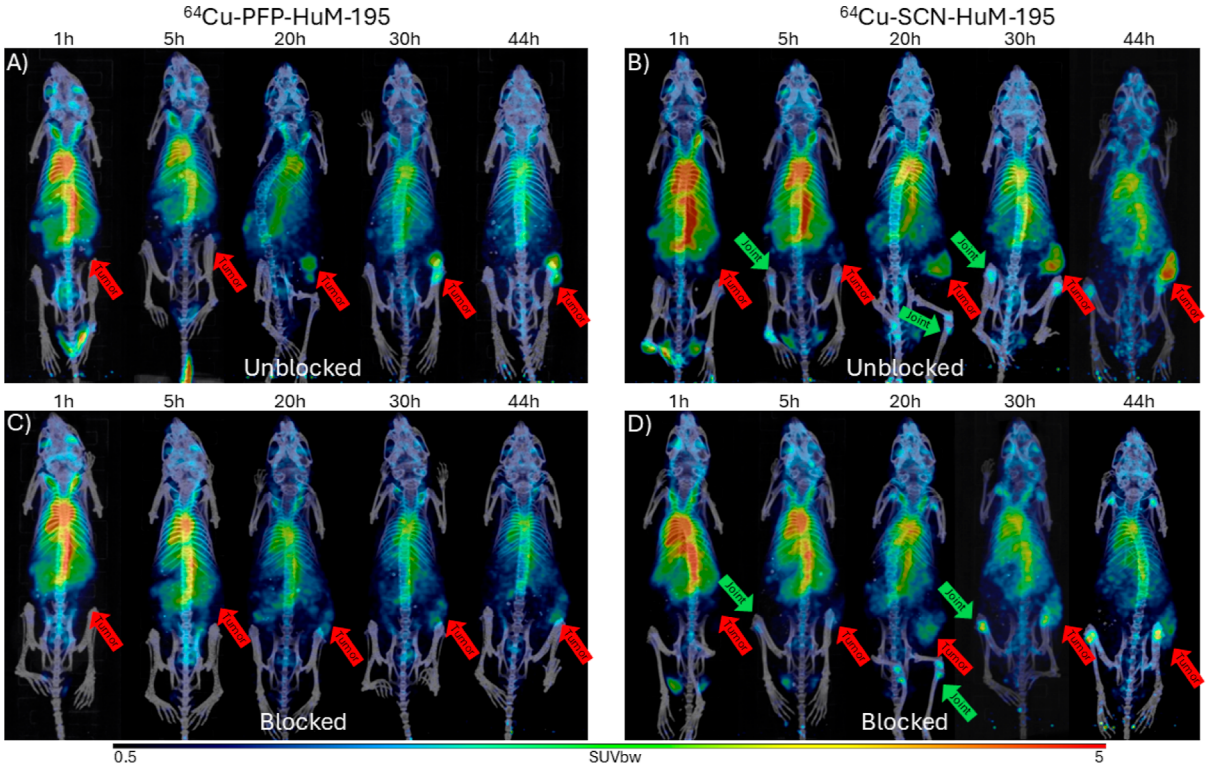

Figure 5. Representative micro-PET/CT images of OCI-AML3 tumor-bearing SCID female mice injected IV with (A) ^{64}Cu-PFP-HuM195 (unblocked), (B) ^{64}Cu-SCN-HuM195 (unblocked), (C) ^{64}Cu-PFP-HuM195 (blocked), and (D) ^{64}Cu−SCN-HuM195 (blocked). Red arrows indicate tumor location. Green arrows indicate radiotracer joint uptake. All images displayed a maximum intensity projection (MIP). Unblocked mice were given only radiolabeled conjugates; blocked mice were given 0.5 mg HuM195 24 h prior to the radioactive dose.

uptake of either blocked or unblocked groups or between conjugation methods. However, at later time points, 20, 30, and 44 h, significantly less radioconjugates were detected in the tumors of the blocked groups, showing that specificity is conserved regardless of the conjugation method (Figure 5 and 7). Interestingly, when examining the images at the 5 h time point, ^{64}Cu−SCN-HuM195 shows uptake in the knee joints for both blocked and unblocked groups (Figure 5B,D); however, this is not observed with ^{64}Cu-PFP-HuM195 (Figure 5A,C). As time progressed, there appears to be more uptake in the joints for the p-SCN-Bn conjugate only. This is likely due to the stability of ^{64}Cu in the DO3A chelator versus DOTA. While DOTA has been reported to have good ^{64}Cu stability, it has been shown to be less stable than the NOTA analogue.[18,19] Recently, it has been shown that while comparing NOTA and DO3A peptide analogues, ^{64}Cu-cunotadipep and ^{64}Cu-cudotadipep, the DO3A analogue was exceedingly stable in mouse serum with a slight increase in stability over the NOTA analogue, though not significant.[20] However, the in vivo stability suggests that the NOTA analogue has a higher stability due to macrocycle size and is able to resist transmetalation more effectively.[21,22] As a direct comparison with current ^{225}Ac RIT treatments (which utilize a DOTA chelator) was desired, DOTA and DO3A were expected to be acceptable for this study. Interestingly, a potential benefit of the site-specific method would be to exploit the recent results of Basuli et al.[23] By using a slightly different SPAAC reagent, they were able to bind ^{89}Zr with a DOTA chelator. This is particularly beneficial for PET imaging as the longer half-life of ^{89}Zr compared to that of ^{64}Cu (78.41 vs 12.7 h) facilitates long-term PET studies without altering the chelator and more accurately representing the longer half-life of ^{225}Ac therapeutics.

Using the micro-PET imaging data of unblocked mice, image-based dosimetry calculations were performed to determine if any significant differences were observed between the two conjugates. Table 2 shows the number of nuclear transitions in human SOs (N_{SO}) calculated for HuM195 conjugates based on the organ uptake scaled values. The results indicate minimal differences between the two HuM195 conjugates: as mentioned above, with the exception of liver uptake, no statistically significant differences in conjugate uptake were observed in the other organs at any time point. Equivalent doses (mSv/MBq) were calculated using the version 2.2.3 of OLINDA software, for both male and female models using the N_{SO} listed in Table 2 as input values. The total number of transitions in the intestine was distributed among the four intestinal sections present in the software, left colon, small intestine, right colon, and rectum, according to their mass ratios relative to the total intestinal mass. In addition, 10% of the blood transitions was assigned to the "heart contents", and the rest was allocated to the "remaining" section since it is assumed that only about 10% of the total blood volume of an adult human is contained in the heart. The results of the organ equivalent doses, calculated by assuming the administration of either ^{177}Lu- or ^{225}Ac-HuM195 conjugates, indicate that PFP-HuM195 generally presented higher dose values (Table 3). However, the dose differences between the two conjugates are minimal. The ratio of tissue dose values of PFP/SCN conjugates labeled with the same radionuclide and using the same model, approaches to one, except for kidney and spleen where the ratio is less than 0.65.

https://doi.org/10.1021/acsomega.4c09450
ACS Omega 2024, 9, 50000−50011

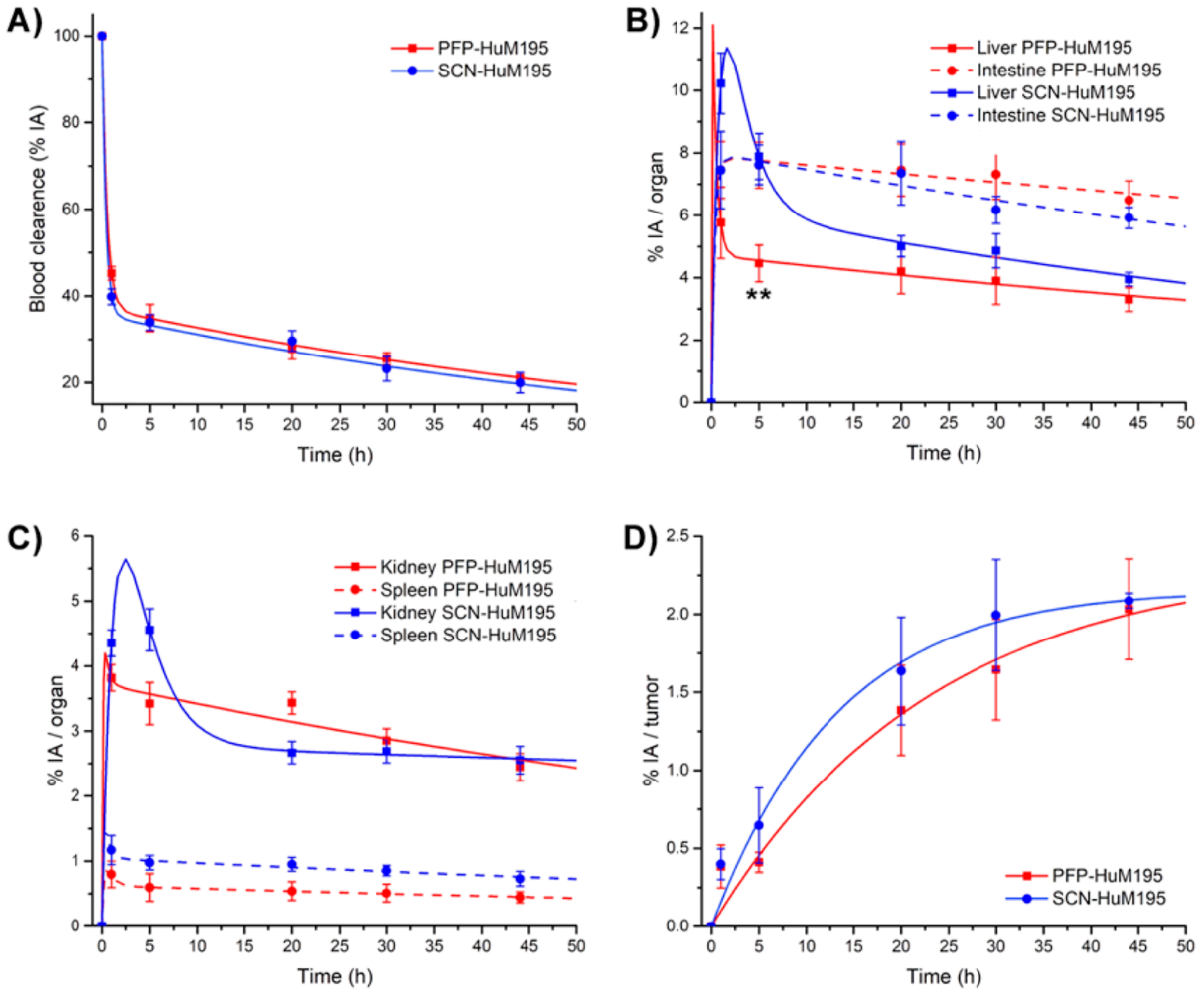

Figure 6. Time−activity curves of the SOs in OCI-AML3 tumor-bearing SCID female mice injected IV with ^{64}Cu−SCN-HuM195 or ^{64}Cu-PFP-HuM195. The curves were obtained from standardized uptake values (SUVs) derived from micro-PET/CT images at different time points. The curves are presented in the following order: (A) blood clearance, (B) liver and intestine activity curves, (C) kidney and spleen activity curves, and (D) tumor kinetic curves.

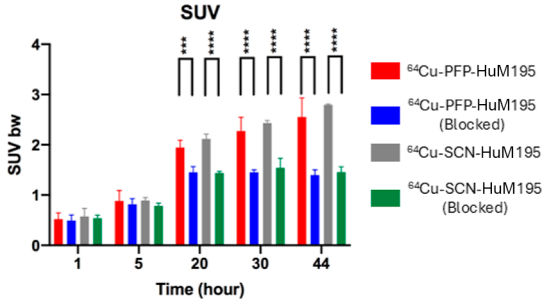

Figure 7. Standardized uptake values normalized by body weight (SUVbw) in OCI-AML3 tumor-bearing SCID female mice injected IV with ^{64}Cu−SCN-HuM195 or ^{64}Cu-PFP-HuM195. Analysis of tumors was based on micro-PET/CT images taken at 1, 5, 20, 30, and 44 h post radioconjugate injection. Tumor region of interest (ROI) was drawn manually for SUV calculations. Significantly more uptake was seen in the unblocked mice starting at 20 h post injection relative to the blocked mice. *** and **** indicate $p < 0.001$ and $p < 0.0001$, respectively. Unblocked mice were given only radiolabeled conjugates; blocked mice were given 0.5 mg HuM195 24 h prior to the radioactive dose.

Greater differences were observed between male and female models using the same conjugate and radionuclide. Comparison of the effective dose values obtained for both ^{177}Lu- and ^{225}Ac-labeled conjugates revealed similar results. These findings suggest that the method of chelator conjugation does not significantly affect the equivalent doses delivered by the labeled antibody to healthy tissues.

Calculated tumor absorbed doses of ^{177}Lu- and ^{225}Ac-HuM195 conjugates, obtained by using sphere models of different sizes, also showed a minimal dose difference between SCN and PFP, but the latter always presents a slightly higher dose with both radionuclides (Table 4). These results also highlight the expected large differences between the absorbed doses produced by the ^{177}Lu-labeled conjugates and those labeled with ^{225}Ac. However, the use of alpha emitters should be carefully evaluated because they also produce from 260 to more than 2000 times the equivalent dose to healthy organs than ^{177}Lu, as shown in Table 3.

There are two limitations of this study. The first one is that HuM195 against human CD33 does not cross-react with murine CD33 which, expressed to some extent on normal B cells, activated T lymphocytes and natural killer cells.[24] The SCID mice, which are widely used for acute myeloid leukemia xenografts including evaluating of radioimmunotherapeutic agents, do not have B or T cells.[25] A second limitation relates

https://doi.org/10.1021/acsomega.4c09450
ACS Omega 2024, 9, 50000−50011

Table 2. Number of Nuclear Transitions Calculated for HuM195 Conjugates in Human Source Organs

source organs	number of nuclear transitions in the source organs (MBq-hr/MBq)							
	^{177}Lu-PFP-HuM195		^{177}Lu-SCN-HuM195		^{225}Ac-PFP-HuM195		^{225}Ac-SCN-HuM195	
	male	female	male	female	male	female	male	female
blood	19.84	20.08	18.25	18.48	21.62	21.88	19.83	20.08
heart	3.49	3.08	3.13	2.77	3.83	3.38	3.40	3.00
liver	2.34	2.21	2.73	2.58	2.67	2.52	3.03	2.87
kidneys	0.80	0.87	1.30	1.41	0.90	0.98	1.69	1.83
spleen	2.73	2.88	4.62	4.36	3.11	3.28	5.27	4.87
intestine	1.21	1.36	0.87	0.96	1.47	1.65	0.99	1.10

Table 3. Equivalent Doses (mSv/MBq) Calculated with the OLINDA v2.2.3 Software for Male and Female ICRP 89 Phantoms Assuming the Administration of HuM195 Conjugates and Their Respective Effective Dose (ED) Using the Organ Weighting Factors Published in ICRP 103

target organ	equivalent doses (mSv/MBq)							
	^{177}Lu-PFP-HuM195		^{177}Lu-SCN-HuM195		^{225}Ac-PFP-HuM195		^{225}Ac-SCN-HuM195	
	male	female	male	female	male	female	male	female
adrenals	3.59×10^{-2}	6.15×10^{-2}	3.90×10^{-2}	7.33×10^{-2}	2.41×10^{1}	3.00×10^{1}	2.22×10^{1}	2.78×10^{1}
brain	2.51×10^{-2}	3.09×10^{-2}	2.31×10^{-2}	2.84×10^{-2}	2.40×10^{1}	2.96×10^{1}	2.21×10^{1}	2.72×10^{1}
breasts		3.15×10^{-2}		2.91×10^{-2}		2.96×10^{1}		2.72×10^{1}
esophagus	3.00×10^{-2}	3.65×10^{-2}	2.83×10^{-2}	3.43×10^{-2}	2.41×10^{1}	2.96×10^{1}	2.21×10^{1}	2.72×10^{1}
eyes	2.51×10^{-2}	3.09×10^{-2}	2.31×10^{-2}	2.85×10^{-2}	2.40×10^{1}	2.96×10^{1}	2.21×10^{1}	2.72×10^{1}
gallbladder wall	3.07×10^{-2}	3.61×10^{-2}	2.93×10^{-2}	3.45×10^{-2}	2.41×10^{1}	2.96×10^{1}	2.21×10^{1}	2.72×10^{1}
left colon	1.09×10^{-1}	1.34×10^{-1}	8.52×10^{-2}	1.05×10^{-1}	2.45×10^{1}	3.02×10^{1}	2.24×10^{1}	2.76×10^{1}
small intestine	1.08×10^{-1}	1.32×10^{-1}	8.35×10^{-2}	1.01×10^{-1}	2.45×10^{1}	3.02×10^{1}	2.24×10^{1}	2.76×10^{1}
stomach wall	3.14×10^{-2}	3.95×10^{-2}	3.09×10^{-2}	3.97×10^{-2}	2.41×10^{1}	2.97×10^{1}	2.21×10^{1}	2.73×10^{1}
right colon	1.08×10^{-1}	1.32×10^{-1}	8.38×10^{-2}	1.01×10^{-1}	2.45×10^{1}	3.02×10^{1}	2.24×10^{1}	2.76×10^{1}
rectum	1.07×10^{-1}	1.30×10^{-1}	8.19×10^{-2}	9.93×10^{-2}	2.45×10^{1}	3.02×10^{1}	2.24×10^{1}	2.76×10^{1}
heart wall	3.31×10^{-1}	4.01×10^{-1}	2.98×10^{-1}	3.62×10^{-1}	3.29×10^{2}	3.99×10^{2}	2.92×10^{2}	3.56×10^{2}
kidneys	2.29×10^{-1}	2.81×10^{-1}	3.71×10^{-1}	4.52×10^{-1}	2.36×10^{2}	2.89×10^{2}	4.42×10^{2}	5.40×10^{2}
liver	1.19×10^{-1}	1.43×10^{-1}	1.38×10^{-1}	1.67×10^{-1}	1.20×10^{2}	1.46×10^{2}	1.37×10^{2}	1.66×10^{2}
lungs	2.85×10^{-2}	3.51×10^{-2}	2.68×10^{-2}	3.28×10^{-2}	2.41×10^{1}	2.96×10^{1}	2.21×10^{1}	2.72×10^{1}
ovaries		3.31×10^{-2}		3.05×10^{-2}		2.96×10^{1}		2.72×10^{1}
pancreas	3.10×10^{-2}	3.78×10^{-2}	2.98×10^{-2}	3.69×10^{-2}	2.41×10^{1}	2.96×10^{1}	2.21×10^{1}	2.72×10^{1}
prostate	2.66×10^{-2}		2.45×10^{-2}		2.40×10^{1}		2.21×10^{1}	
salivary glands	2.56×10^{-2}	3.11×10^{-2}	2.36×10^{-2}	2.86×10^{-2}	2.40×10^{1}	2.96×10^{1}	2.21×10^{1}	2.72×10^{1}
red marrow	2.08×10^{-2}	2.53×10^{-2}	1.96×10^{-2}	2.36×10^{-2}	2.78×10^{1}	3.39×10^{1}	2.55×10^{1}	3.11×10^{1}
osteogenic cells	3.02×10^{-2}	2.92×10^{-2}	2.83×10^{-2}	2.73×10^{-2}	9.24×10^{1}	8.39×10^{1}	8.48×10^{1}	7.69×10^{1}
spleen	1.57×10^{0}	1.91×10^{0}	2.66×10^{0}	2.89×10^{0}	1.68×10^{3}	2.05×10^{3}	2.85×10^{3}	3.04×10^{3}
testes	2.52×10^{-2}		2.32×10^{-2}		2.40×10^{1}		2.21×10^{1}	
thymus	3.01×10^{-2}	3.58×10^{-2}	2.78×10^{-2}	3.31×10^{-2}	2.41×10^{1}	2.96×10^{1}	2.21×10^{1}	2.72×10^{1}
thyroid	2.63×10^{-2}	3.19×10^{-2}	2.43×10^{-2}	2.94×10^{-2}	2.40×10^{1}	2.96×10^{1}	2.21×10^{1}	2.72×10^{1}
urinary bladder wall	2.63×10^{-2}	3.26×10^{-2}	2.42×10^{-2}	2.99×10^{-2}	2.40×10^{1}	2.96×10^{1}	2.21×10^{1}	2.72×10^{1}
uterus		3.34×10^{-2}		3.06×10^{-2}		2.96×10^{1}		2.72×10^{1}
total body	3.83×10^{-2}	4.74×10^{-2}	3.89×10^{-2}	4.76×10^{-2}	3.59×10^{1}	4.37×10^{1}	3.70×10^{1}	4.44×10^{1}
ED	5.45×10^{-2}	7.06×10^{-2}	6.24×10^{-2}	7.67×10^{-2}	4.41×10^{1}	5.72×10^{1}	5.55×10^{1}	6.70×10^{1}

Table 4. Absorbed Doses (Gy/MBq) Calculated with OLINDA v2.2.3 Software for Unit-Density Spheres of Different Sizes Simulating the Administration of HuM195 Conjugates

sphere diameter [mm]	sphere mass [g]	PFP-HuM195		SCN-HuM195	
		^{177}Lu (Gy/MBq)	^{225}Ac (Gy/MBq)	^{177}Lu (Gy/MBq)	^{225}Ac (Gy/MBq)
2.7	0.01	35.0	52156.2	33.5	49246.4
5.8	0.1	36.5	52197.2	34.9	49285.2
12.4	1	37.4	52218.2	35.7	49305.0

to the dosimetric studies as they were conducted based on the assumption that the biodistribution profile of HuM195 conjugates labeled with ^{177}Lu and ^{225}Ac would be identical to that of the ^{64}Cu-conjugates. However, it is well-established that each metal ion has specific chemical requirements due to intrinsic properties such as atomic number, charge, and radius. These characteristics lead to distinct preferences for ligand donor atoms, coordination numbers, and geometries, which can influence the physicochemical properties and, consequently, the biodistribution profile of each metal complex.

https://doi.org/10.1021/acsomega.4c09450
ACS Omega 2024, 9, 50000−50011

Despite this, the assumption was made since the primary goal of this study was not to achieve precise dosimetry but rather to provide a preliminary comparison between the two conjugation routes. Further studies with HuM195 conjugates labeled effectively with ^{177}Lu and ^{225}Ac are necessary to determine accurately the organs' absorbed dose.

EXPERIMENTAL PROCEDURES

Reagents and Radionuclides. HuM195 anti-CD33 recombinant antibody (lintuzumab) (CAT#: TAB-756) was purchased from Creative Biolabs (Shirley, NY, USA). ^{225}Ac was purchased from Oak Ridge National Laboratory, TN, USA. ^{177}Lu was acquired from McMaster University (Hamilton, ON, Canada), and ^{64}Cu was acquired from the University of Alberta (Edmonton, AB, Canada). All other reagents were purchased from Fisher Scientific (Ottawa, ON, Canada) unless otherwise stated. All buffers used for conjugation and radiolabeling were passed through a Chelex-100 cation exchange resin to remove any adventitious metals.

Cell Culture. Human CD33$^+$ acute myeloid leukemia cells (OCI-AML3) and human CD33$^-$ Burkitt's lymphoma cells (Daudi) were obtained from Leibniz Institute DSMZ GmbH (Braunschweig, Germany) and ATCC (Rockville, MD), respectively. Both cell lines were maintained in complete culture medium (RPMI 1640 + 10% fetal bovine serum; R8758 Sigma-Aldrich, SH30088.03, Cytiva) in an incubator at 37 °C with 5% CO_2.

Conjugation. SCN-HuM195: HuM195 was conjugated via a previously described method[26] using a 10 and 20 M excess of p-SCN-Bn-DOTA (Macrocyclics, Plano, TX, USA) resulting in SCN-HuM195. MALDI-TOF MS analysis (University of Alberta) determined a CAR of 4.5 and 8.7 for the 10 and 20 M excess of p-SCN-Bn-DOTA, respectively.

PFP-HuM195: PFP-HuM195 was synthesized using a modified literature procedure;[5] in short, 0.5 mg HuM195 was added to 100 μL of PBS and cooled to 0 °C in ice. To this was added 2.53 μL of a 10 mg/mL solution of azido-PEG8-PFP-Ester (BroadPharm, San Diego, CA, USA) dissolved in cold DMF to afford a 12 molar excess of the PFP-ester over the antibody. This solution was then placed on a prechilled shaker at 4 °C in a "cold" room overnight while shaking at 666 rpm. After the reaction time, the mixture was placed back on ice, and 0.01 M HCl was added until the pH reached between 5.6 and 5.8. The solution was then added to a 30,000 MWC Amicon filter and washed 10× using PBS. A 100 mg/mL solution of DO3A-DBCO (Macrocyclics, Plano, TX, USA) in DMF was freshly made, and 2.6 μL (100 equiv) was added into the purified antibody solution. This reaction mixture was left shaking at room temperature overnight. The antibody was then washed using a 30k MWC Amicon filter 10× into 0.15 M ammonium acetate buffer (pH 6.5). MALDI-TOF MS analysis (University of Alberta) determined a CAR of 2.4.

Internalization of Conjugated Antibodies. OCI-AML3 cells were cultured in RPMI 1640 supplemented with 10% fetal bovine serum and maintained at 37°C + 5% CO_2. 1.0 × 10^6 cells were aliquoted in triplicate into Eppendorf tubes and incubated on ice with 1 mL of 5 μg/mL HuM195, HuM195-PFP, HuM195-SCN, or IgG-DOTA in complete medium. Cells were washed 3× with ice-cold PBS and resuspended in prewarmed complete medium and plated in a 96-well flat bottom culture plate (Thermo Scientific, Cat#167008). At 3, 6, 18, and 24 h post antibody incubation, cells were removed and washed 2× with flow cytometry buffer (PBS +2% FBS +0.02% sodium azide). Cells were stained with 2.5 μg/mL goat antihuman IgG-PE (Invitrogen, Cat#12-4998-82) for 30 min on ice. Cells were washed 3× with flow cytometry buffer, and data were collected on a Beckman Coulter CytoFlex instrument. Data were analyzed with FlowJo software version 10.4.1.

Radiolabeling and Stability Studies. Both antibody conjugates were labeled in a similar manner as previously described.[25] In short, ^{177}Lu or ^{64}Cu were mixed with the conjugated antibody with a specific activity of 0.185:1 or 0.37:1 MBq/μg antibody (5:1 or 10:1 μCi/μg). For ^{225}Ac-radiolabeling a 0.037:1 MBq/μg (1:1 μCi/μg) specific activity was utilized. Labeling was carried out at 37 °C for 1 h with shaking and quenched with either 3 μL of 50 mM EDTA or DTPA solution. All yields were >95% measured via instant thin layer chromatography (iTLC) by cutting the iTLC strips in half and measuring the radioactivity of the top part of the strip (unbound radioisotope) versus the bottom part (antibody bound radioisotope) on a Wizard 2470 gamma counter (PerkinElmer, Waltham, MA, USA). RadioHPLC (Agilent Technologies, Santa Clara, CA, USA) was performed to confirm attachment of the radioisotope to the antibody and the antibody intactness post radiolabeling.

To evaluate the stability of the radiolabeled antibodies, they were labeled with ^{225}Ac and purified via spin filtration (3×) using an Amicon 30k MWC filter into PBS. iTLC was immediately run after purification to give a purity of >99%. The radiolabeled antibody was then split into two groups: one containing only PBS, and to the other group, human serum was added so that the solution contained 90% human serum and 10% PBS. Samples were then placed in an incubator at 37 °C. At the predetermined time points (24, 48, and 168 h), a 5 μL aliquot was removed and added to 5 μL of 0.15 M ammonium acetate, followed by 2 μL of 50 mM DTPA solution. The mixture was allowed to sit for 5 min before an iTLC was ran in triplicate as described above.

Animal Models. All animal experiments were approved by the University of Saskatchewan Animal Research Ethics Board (Protocol number: 20,170,006) in accordance with the Canadian Council of Animal Care guidelines. Human tumor xenografts were established in 6 week old female Fox Chase SCID mice (Strain code: 236, Charles River laboratories, Saint-Constant, QC, Canada). OCI-AML3 cells were prepared for injection in a 1:1 ratio of Cultrex Reduced Growth Factor Basement Membrane Extract (R&D Systems, Minneapolis, MN, USA) and complete growth medium. 2 ×10^6 OCI-AML3 in 100 μL was then injected subcutaneously into the right flank of SCID mice. Tumor growth was measured with an electronic caliper every 3 days. On day 14 post tumor inoculation, tumor reached the average size of about 200 mm^3.

ELISA. Corning High Binding 96-well plate (Cat#9018, Corning, NY, USA) was coated with 0.1 μg/well of recombinant human Siglec-3 (CD33, SinoBiologicals Cat# 12238-HCCH) in carbonate/bicarbonate coating buffer (100 mM, pH 9.6) overnight at 4 °C. The plate was washed with PBS +0.1% Tween20 (PBST), blocked with 0.5% BSA in PBST (blocking buffer) for 1.5 h at room temperature. The plate was then incubated with 1:10 serial dilutions of HuM195 immunoconjugates from 6.6 to 6.6 × 10^{-7} μM in blocking buffer for 1.5 h at room temperature (n = 3/immunoconjugate, n = 2 for control IgG). Secondary antibody (goat anti-human kappa HRP, Invitrogen, Catalog # A18853) was added to wells at 1:10,000 dilution in blocking buffer for 1.5 h at RT. The

https://doi.org/10.1021/acsomega.4c09450
ACS Omega 2024, 9, 50000−50011

plate was developed after addition of the TMB substrate (Thermo Fisher, Cat#34021) for 10 min protected from light. The reaction was stopped with 1 M HCl and read on a Spectramax 250 microplate reader (Molecular Devices, Cat#MD-S250) at 450 nm. Data were analyzed and graphed using GraphPad Prism (Version 7.04, GraphPad Software Inc., Boston, MA, USA).

Cytotoxicity Assay. $CD33^+$ OCI-AML3 cells plated at 1.5×10^4 cells in 0.5% bovine serum albumin/PBS overnight blocked 96 V-bottom plates (Catalog# AK701201, AAKA Scientific, Edmonton, AB). Cells were incubated in 100 μL of complete medium supplemented with decreasing doses of 0.037:1 MBq/μg specific activity labeled ^{225}Ac-DOTA-HuM195 immunoconjugates (185−0.36 kBq/mL, n = 3/treatment) for 3 h at 37°C + 5% CO_2 with gentle agitation. Cells were then washed 3 times with sterile PBS, resuspended in complete medium supplemented with 250 nM of Incucyte Cytotox Red Dye (catalogue no. 4632, Sartorius, Gottingen, Germany), and plated in a dry clear 96-well flat bottom plate (catalogue no. 353072, Corning, NY, USA) precoated with 0.01% poly-*L*-ornithine solution. Images were captured every 30 min for 24 h using an Incucyte S3 Live Cell Analysis Instrument (Sartorius). Raw image data were collected from 4 images per well of three independently treated samples per time point. Data were then analyzed by plotting the average of total red object area of the 4 images/well per time point (n = 3/treatment).

Flow Cytometry. 2.5×10^5 $CD33^+$ OCI-AML3 cells or $CD33^-$ Daudi were plated in a Nunc 96-Well U bottom plate (Cat#267245, Thermo Fisher). Cells were washed using FACS buffer (PBS +2% FBS +0.02% sodium azide) and stained with 1:10 serial dilutions (0.1 to 0.1×10^{-9} mg/mL) of p-SCN-Bn or PFP HuM195 immunoconjugates (n = 3/conjugate, n = 2/conjugate for Daudi cell line) for 1 h at 4 °C. Cells were subsequently washed with buffer and stained with 0.5 μg/well of eBioscience Goat antihuman IgG PE conjugated secondary (cat# 12-4998-82, Thermo Fisher) for 30 min at 4 °C. Data were collected on a Beckman Coulter CytoFlex instrument and analyzed with FloJo (Version 10.4.1, BD Bioscience, Franklin Lakes, NJ, USA). Data are presented as the mean fluorescence intensity (MFI) of the *R*-phycoerythrin channel (575/26 nm).

Micro-PET/CT Imaging. Mice (n = 16) were injected with 313 ± 8 μCi (11.6 ± 0.3 MBq) of ^{64}Cu-labeled antibody and imaged at 1, 5, 20, 30, and 44 h post injection. Blocked mice (n = 8) were injected with 0.5 mg of HuM195 24 h prior to the radioactive dose. Micro-PET/CT data were collected on a GNEXT micro-PET/CT scanner (Xodus Imaging, Dulles, VA, USA). Mice were scanned for 10 min (static) for the 1, 5, and 20 h scan and for 20 min for the 30 and 44 h scan. Animals in each group (n = 4) were scanned simultaneously using a multimouse bed. After the last scan (44 h), mice were sacrificed and an ex vivo biodistribution study was performed. Blood and selected organs were collected and measured using a 2470 Wizard2 Gamma counter to calculate the percent of injected activity per gram (% IA/g) of tissue.

The micro-PET/CT images were automatically registered and reconstructed using the GNEXT system. PET images were reconstructed using a three-dimensional ordered subset expectation maximization (3D-OSEM) algorithm, which employed 24 subsets and 3 iterations, while CT images were reconstructed using a modified Feldkamp algorithm. The volumes of interest (VOIs) for the SOs and the whole body were delineated manually on the CT images at each time point and subsequently applied to the corresponding PET images to obtain the activity within the VOIs, using P-MOD v4.101 software (Zurich, Switzerland). The aforementioned activity values, along with the weight of each mouse, the injected activity, the time of administration, and the acquisition time (for decay correction), were utilized to calculate SUVs, which were expressed as % IA/g. Finally, the resulting decay-corrected % IA/g values were used to generate the kinetic curves of the SO for both ADCs. The blood concentrations of HuM195 conjugates at each time point were calculated as the product of the % IA per gram in the heart (caused by the activity in the blood contained in this organ) by the blood weight (8% of the mouse weight). This value was used to obtain the blood clearance curve. Maximum intensity projection (MIP) images were generated to visualize tumor uptake, and tumor VOIs were delineated directly on the PET images to determine the activity within the VOIs.

Dosimetry. Human dosimetry calculations were performed for both p-SCN-Bn and PFP conjugates, assuming that they were labeled with the therapeutic radionuclides ^{177}Lu or ^{225}Ac. First, the values of % IA/g of tissue obtained for each time point were scaled from mice to humans using male or female models, according to the following formula

$$\left(\frac{\%\ \mathrm{IA}}{\mathrm{organ}}\right)_{\mathrm{H}} = \left(\frac{\%\ \mathrm{IA}}{\mathrm{g}}\right)_{\mathrm{M}} \times \frac{\mathrm{OW_H}}{\mathrm{TBW_H}} \times \mathrm{TBW_M}$$

where OW_H represents the weight of the human organ, while TBW_H and TBW_M correspond to the average total body weight of humans and mice, respectively. The OW_H and TBW_H values were obtained for male and female models from the phantoms reported in ICRP 89.[27]

The decay-corrected percentage of the injected activity per gram of tissue (IA/g) values calculated for the human models was plotted as a function of the postinjection time in order to obtain the organ activity curves. Subsequently, the N_{SO} (MBq-hr/MBq) per MBq of the ^{177}Lu- or ^{225}Ac-labeled conjugates was determined using the CoKiMo software,[28] which fitted the obtained organ activity curves to a triexponential equation, corrected them for the physical decay of each radionuclide, and integrated them up to five radionuclide half-lives.

The dose calculations were performed with the OLINDA software, code version 2.2.3,[29] using as input the N_{SO} per unit of administered activity previously calculated and the male or female human adult realistic NURBS-type models. To obtain the equivalent doses to normal organs and tissues, the absorbed doses attributed to alpha emissions were multiplied by a radiation weighting factor of 5. The organ absorbed dose generated by ^{225}Ac was calculated by adding the contributions of the daughter radionuclides, taking into account their branching ratio.

Tumor absorbed dose calculations were performed using the "Sphere model" of the OLINDA software to obtain the self-dose to spheres of unit density of different sizes. The number of nuclear transitions (MBq-h/MBq) in the spheres was calculated for both HuM195 conjugates labeled with ^{177}Lu or ^{225}Ac, by integrating the % IA/g curve obtained by imaging analysis, taking into account the physical decay of each radionuclide. The tumor absorbed dose generated by ^{225}Ac was calculated as mentioned before adding the contributions of the daughter radionuclides. In this case, only the tumor absorbed doses were calculated, and therefore, the values were not

https://doi.org/10.1021/acsomega.4c09450
ACS Omega 2024, 9, 50000−50011

multiplied by the alpha radiation weighting factor required to determine the equivalent doses.

Statistical Analysis. Data were analyzed and graphed using GraphPad Prism (Version 7.04, GraphPad Software Inc., Boston, MA, USA). All graphs are presented as mean ± SD. For ELISA and flow cytometry data, concentrations (μM) were log transformed and analyzed using Sigmoidal 4PL analysis, where X is the log (concentration) function to obtain K_d and EC_{50} values. In vitro cytotoxicity was analyzed using ordinary one-way ANOVA with multiple comparison. The biodistribution at different time points was analyzed by a multiple paired *t*-test for each organ. *P*-values presented as ≥0.05 (n.s.), ≤0.05 (*), ≤0.002 (**), ≤0.0002 (***), and ≤0.0001 (****).

CONCLUSIONS

In this study, we evaluated two antibody conjugation methods to enable downstream radiolabeling: PFP that selectively attaches chelators onto the conserved K188 residue of IgG1 antibodies and a p-SCN-Bn random conjugation method that targets available lysine residues. Using several clinically relevant radioisotopes, we assessed their viability in the resulting conjugates for future clinical work. Both methods were highly reliable with commercially available materials and achieved excellent radioisotope incorporation without significant differences. Some difference in multiday stability were observed; however, both methods showed reliable radioisotopic retention. In vitro binding experiments showed a significant decrease in Bmax for the p-SCN-Bn conjugate as well as slightly less pronounced cytotoxicity, which may be due to the decrease in binding capacity. Pharmacokinetic and dosimetry analyses revealed that there was slightly higher uptake in the liver for the p-SCN-Bn conjugate, while no significant differences were observed for any other healthy organ or acute myeloid leukemia tumors. While both methods are viable for future work, the PFP site-specific method offers potential advantages such as pretargeting.[8,30]

ASSOCIATED CONTENT

Supporting Information

The Supporting Information is available free of charge at https://pubs.acs.org/doi/10.1021/acsomega.4c09450.

Flow cytometry of antibody conjugates binding to CD33+ and control cells; Incucyte images of cells treated with ^{225}Ac-labeled antibodies; and ex vivo biodistribution data from mice injected with ^{64}Cu-labeled antibodies (PDF)

AUTHOR INFORMATION

Corresponding Author

Ekaterina Dadachova − *College of Pharmacy and Nutrition, University of Saskatchewan, Saskatoon, Saskatchewan S7N 5E5, Canada;* orcid.org/0000-0001-7300-6479; Phone: 1-306-966-5163; Email: ekaterina.dadachova@usask.ca

Authors

Kevin J. H. Allen − *College of Pharmacy and Nutrition, University of Saskatchewan, Saskatoon, Saskatchewan S7N 5E5, Canada*

Connor Frank − *College of Pharmacy and Nutrition, University of Saskatchewan, Saskatoon, Saskatchewan S7N 5E5, Canada*

Rubin Jiao − *College of Pharmacy and Nutrition, University of Saskatchewan, Saskatoon, Saskatchewan S7N 5E5, Canada*

Mackenzie E. Malo − *College of Pharmacy and Nutrition, University of Saskatchewan, Saskatoon, Saskatchewan S7N 5E5, Canada*

Michele Bello − *Department of Physics and Astronomy, University of Padua, Padua I-35131, Italy*

Laura De Nardo − *Department of Physics and Astronomy, University of Padua, Padua I-35131, Italy;* orcid.org/0000-0002-0061-370X

Laura Meléndez-Alafort − *Immunology and Molecular Oncology Diagnostics Unit, Veneto Institute of Oncology IOV-IRCCS, Padua 35128, Italy;* orcid.org/0000-0003-0701-3616

Complete contact information is available at: https://pubs.acs.org/10.1021/acsomega.4c09450

Author Contributions

‖K.J.H.A. and C.F. contributed equally to this work.

Notes

The authors declare no competing financial interest.

ACKNOWLEDGMENTS

This work was carried out as part of the activities of the Coordinated Research Project F-22078 funded by the IAEA.

REFERENCES

(1) Larson, S. M.; Carrasquillo, J. A.; Cheung, N.-K. V.; Press, O. W. Radioimmunotherapy of human tumours. *Nat. Rev. Cancer* **2015**, *15* (6), 347−360.

(2) Agarwal, P.; Bertozzi, C. R. Site-Specific Antibody−Drug Conjugates: The Nexus of Bioorthogonal Chemistry, Protein Engineering, and Drug Development. *Bioconjugate Chem.* **2015**, *26* (2), 176−192.

(3) Anami, Y.; Xiong, W.; Gui, X.; Deng, M.; Zhang, C. C.; Zhang, N.; An, Z.; Tsuchikama, K. Enzymatic conjugation using branched linkers for constructing homogeneous antibody−drug conjugates with high potency. *Org. Biomol. Chem.* **2017**, *15* (26), 5635−5642.

(4) El Alaoui, M.; Sivado, E.; Jallas, A.-C.; Mebarki, L.; Dyson, M. R.; Perrez, F.; Valsesia-Wittmann, S.; El Alaoui, S. Antibody and antibody fragments site-specific conjugation using new Q-tag substrate of bacterial transglutaminase. *Cell Death Discov.* **2024**, *10* (1), 79.

(5) Sarrett, S. M.; Rodriguez, C.; Rymarczyk, G.; Hosny, M. M.; Keinänen, O.; Delaney, S.; Thau, S.; Krantz, B. A.; Zeglis, B. M. Lysine-Directed Site-Selective Bioconjugation for the Creation of Radioimmunoconjugates. *Bioconjugate Chem.* **2022**, *33* (9), 1750−1760.

(6) Pham, G. H.; Ou, W.; Bursulaya, B.; DiDonato, M.; Herath, A.; Jin, Y.; Hao, X.; Loren, J.; Spraggon, G.; Brock, A.; Uno, T.; Geierstanger, B. H.; Cellitti, S. E. Tuning a Protein-Labeling Reaction to Achieve Highly Site Selective Lysine Conjugation. *ChemBioChem* **2018**, *19* (8), 799−804.

(7) Bhat, A. S. B. C. W.; Lareunt, O. A.; Lee, A.; Presston, R. R.; Tumelty, D.; Wood, L. D.; Yu, W. H. Multifunctional antibody conjugates. US20120201809A1, 2014.

(8) Bauer, D.; Cornejo, M. A.; Hoang, T. T.; Lewis, J. S.; Zeglis, B. M. Click Chemistry and Radiochemistry: An Update. *Bioconjugate Chem.* **2023**, *34* (11), 1925−1950.

(9) Kristensen, L. K.; Christensen, C.; Jensen, M. M.; Agnew, B. J.; Schjöth-Frydendahl, C.; Kjaer, A.; Nielsen, C. H. Site-specifically labeled (89)Zr-DFO-trastuzumab improves immuno-reactivity and

tumor uptake for immuno-PET in a subcutaneous HER2-positive xenograft mouse model. *Theranostics* **2019**, *9* (15), 4409−4420.
(10) Sadiki, A.; Kercher, E. M.; Lu, H.; Lang, R. T.; Spring, B. Q.; Zhou, Z. S. Site-specific Bioconjugation and Convergent Click Chemistry Enhances Antibody-Chromophore Conjugate Binding Efficiency. *Photochem. Photobiol.* **2020**, *96* (3), 596−603.
(11) Sudo, H.; Tsuji, A. B.; Sugyo, A.; Harada, Y.; Nagayama, S.; Katagiri, T.; Nakamura, Y.; Higashi, T. Head-to-head comparison of three chelates reveals DOTAGA promising for (225) Ac labeling of anti-FZD10 antibody OTSA101. *Cancer Sci.* **2023**, *114* (12), 4677−4690.
(12) Jurcic, J. G. Ab therapy of AML: native anti-CD33 Ab and drug conjugates. *Cytotherapy* **2008**, *10* (1), 7−12.
(13) Jurcic, J. G. Targeted Alpha-Particle Therapy for Hematologic Malignancies. *Semin Nucl. Med.* **2020**, *50* (2), 152−161.
(14) Rosenblat, T. L.; McDevitt, M. R.; Carrasquillo, J. A.; Pandit-Taskar, N.; Frattini, M. G.; Maslak, P. G.; Park, J. H.; Douer, D.; Cicic, D.; Larson, S. M.; Scheinberg, D. A.; Jurcic, J. G. Treatment of Patients with Acute Myeloid Leukemia with the Targeted Alpha-Particle Nanogenerator Actinium-225-Lintuzumab. *Clin. Cancer Res.* **2022**, *28* (10), 2030−2037.
(15) Ma, J.; Li, L.; Liao, T.; Gong, W.; Zhang, C. Efficacy and Safety of (225)Ac-PSMA-617-Targeted Alpha Therapy in Metastatic Castration-Resistant Prostate Cancer: A Systematic Review and Meta-Analysis. *Front Oncol* **2022**, *12*, 796657.
(16) Sathekge, M.; Bruchertseifer, F.; Vorster, M.; Lawal, I. O.; Knoesen, O.; Mahapane, J.; Davis, C.; Mdlophane, A.; Maes, A.; Mokoala, K.; Mathabe, K.; Van, C.; Wiele, D.; Morgenstern, A. mCRPC Patients Receiving (225)Ac-PSMA-617 Therapy in the Post-Androgen Deprivation Therapy Setting: Response to Treatment and Survival Analysis. *J. Nucl. Med.* **2022**, *63* (10), 1496−1502.
(17) Kittel-Boselli, E.; Soto, K. E. G.; Loureiro, L. R.; Hoffmann, A.; Bergmann, R.; Arndt, C.; Koristka, S.; Mitwasi, N.; Kegler, A.; Bartsch, T.; Berndt, N.; Altmann, H.; Fasslrinner, F.; Bornhäuser, M.; Bachmann, M. P.; Feldmann, A. Targeting Acute Myeloid Leukemia Using the RevCAR Platform: A Programmable, Switchable and Combinatorial Strategy. *Cancers* **2021**, *13* (19), 4785.
(18) Woo, S. K.; Jang, S. J.; Seo, M. J.; Park, J. H.; Kim, B. S.; Kim, E. J.; Lee, Y. J.; Lee, T. S.; An, G. I.; Song, I. H.; Seo, Y.; Kim, K. I.; Kang, J. H. Development of (64)Cu-NOTA-Trastuzumab for HER2 Targeting: A Radiopharmaceutical with Improved Pharmacokinetics for Human Studies. *J. Nucl. Med.* **2019**, *60* (1), 26−33.
(19) Qiao, Z.; Xu, J.; Gonzalez, R.; Miao, Y. Novel 64Cu-Labeled NOTA-Conjugated Lactam-Cyclized Alpha-Melanocyte-Stimulating Hormone Peptides with Enhanced Tumor to Kidney Uptake Ratios. *Mol. Pharmaceutics* **2022**, *19* (7), 2535−2541.
(20) Lee, I.; Kim, M. H.; Lee, K.; Oh, K.; Lim, H.; Ahn, J. H.; Lee, Y. J.; Cheon, G. J.; Chi, D. Y.; Lim, S. M. Comparison of the Effects of DOTA and NOTA Chelators on (64)Cu-Cudotadipep and (64)Cu-Cunotadipep for Prostate Cancer. *Diagnostics* **2023**, *13* (16), 2649.
(21) Prasanphanich, A. F.; Nanda, P. K.; Rold, T. L.; Ma, L.; Lewis, M. R.; Garrison, J. C.; Hoffman, T. J.; Sieckman, G. L.; Figueroa, S. D.; Smith, C. J. [64Cu-NOTA-8-Aoc-BBN(7−14)NH2] targeting vector for positron-emission tomography imaging of gastrin-releasing peptide receptor-expressing tissues. *Proc. Natl. Acad. Sci. U.S.A.* **2007**, *104* (30), 12462−12467.
(22) Boswell, C. A.; Sun, X.; Niu, W.; Weisman, G. R.; Wong, E. H.; Rheingold, A. L.; Anderson, C. J. Comparative in vivo stability of copper-64-labeled cross-bridged and conventional tetraazamacrocyclic complexes. *J. Med. Chem.* **2004**, *47* (6), 1465−1474.
(23) Basuli, F.; Vasalatiy, O.; Shi, J.; Lane, K. C.; Escorcia, F. E.; Swenson, R. E. Preparation of a Zirconium-89 Labeled Clickable DOTA Complex and Its Antibody Conjugate. *Pharmaceuticals* **2024**, *17* (4), 480.
(24) Samadani, A. A.; Keymoradzdeh, A.; Shams, S.; Soleymanpour, A.; Rashidy-Pour, A.; Hashemian, H.; Vahidi, S.; Norollahi, S. E. CAR T-cells profiling in carcinogenesis and tumorigenesis: An overview of CAR T-cells cancer therapy. *Int. Immunopharmacol.* **2021**, *90*, 107201.
(25) Hagemann, U. B.; Wickstroem, K.; Wang, E.; Shea, A. O.; Sponheim, K.; Karlsson, J.; Bjerke, R. M.; Ryan, O. B.; Cuthbertson, A. S. Vitro and In Vivo Efficacy of a Novel CD33-Targeted Thorium-227 Conjugate for the Treatment of Acute Myeloid Leukemia. *Mol. Cancer Ther.* **2016**, *15* (10), 2422−2431.
(26) Garg, R.; Allen, K. J. H.; Dawicki, W.; Geoghegan, E. M.; Ludwig, D. L.; Dadachova, E. 225Ac-labeled CD33-targeting antibody reverses resistance to Bcl-2 inhibitor venetoclax in acute myeloid leukemia models. *Cancer Med.* **2021**, *10* (3), 1128−1140.
(27) Basic anatomical and physiological data for use in radiological protection: reference values. A report of age- and gender-related differences in the anatomical and physiological characteristics of reference individuals. ICRP Publication 89. *Ann. ICRP* **2002**, *32* (3−4), 5−265.
(28) Meléndez-Alafort, L.; Rosato, A.; Ferro-Flores, G.; Penev, I.; Uzunov, N. Development of a five-compartmental model and software for pharmacokinetic studies. *Comptes Rendus de L'Academie Bulgare des Sciences* **2017**, *70* (12), 1649−1654.
(29) Stabin, M.; Farmer, A. OLINDA/EXM 2.0: The new generation dosimetry modeling code. *J. Nucl. Med.* **2012**, *53* (supplement 1), 585.
(30) Cheal, S. M.; Chung, S. K.; Vaughn, B. A.; Cheung, N.-K. V.; Larson, S. M. Pretargeting: A Path Forward for Radioimmunotherapy. *J. Nucl. Med.* **2022**, *63* (9), 1302−1315.

https://doi.org/10.1021/acsomega.4c09450
ACS Omega 2024, 9, 50000−50011